A Multidimensional Omics Approach Reveals Biased Signaling Through a flg22- and UDP-glucose-Induced, AtRGS1-driven Signaling Circuit

Zhi Li[1, 2], Eduardo Simoni[1,3], Jing Yang[1], Christian Montes[2], Justin W. Walley[2*], Alan M. Jones[1,4]

[1]Department of Biology, University of North Carolina, Chapel Hill, NC 27599 USA

[2]Department of Plant Pathology, Entomology, and Microbiology, Iowa State University, Ames Iowa, 50011 USA

[3]Department of Biochemistry and Molecular Biology, BIOAGRO, Universidade Federal de Viçosa, Viçosa, MG 36570-900, Brazil

[4]Department of Pharmacology, University of North Carolina, Chapel Hill, NC 27599 USA

[*]Correspondence to: jwalley@iastate.edu

Supplementary Information S1. Data showing UDPG and flg22 induce rapid phosphorylation of AtRGS1 *in vivo* with different decay times. This figure supports text in the introduction. The following data is reproduced here with permission. UDPG-induced phosphorylation of AtRGS1 (left immunoblot) is taken from Jia et al[1]. flg22 induced phosphorylation of AtRGS1 (right immunoblot) is taken from Watkins, et al paper[2].

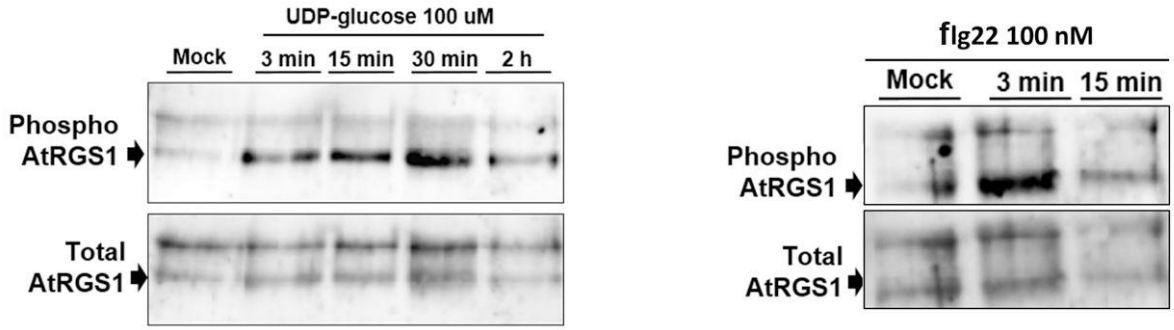


Figure S1. Both flg22 and UDPG induce AtRGS1 phosphorylation within 3 minutes. AtRGS1 was expressed in cells as described for the UDP-glucose treatment (left) in Jia et al[1] and for the flg22 treatment (right) in Watkins et al[2]. These publications also describe how purified IGG to the phosphorylated peptide corresponding to the phosphocluster (aa 428-436) were used to detect AtRGS1 phosphorylation induced by UDP-glucose and flg22. Total AtRGS1 was detected with polyclonal sera to ATRGS1 as described.

Supplemental Information S2. This data supports data shown in Figure 1H. The design of these experiments was based on the data shown in Figure S2. The purpose of Panel A is to provide the negative control for ROS production using the flg22 receptor null mutant, fls2. The purpose on panel B is to show that UDPG does induce a small ROS burst but only detectable in the rgs1-2 mutant.

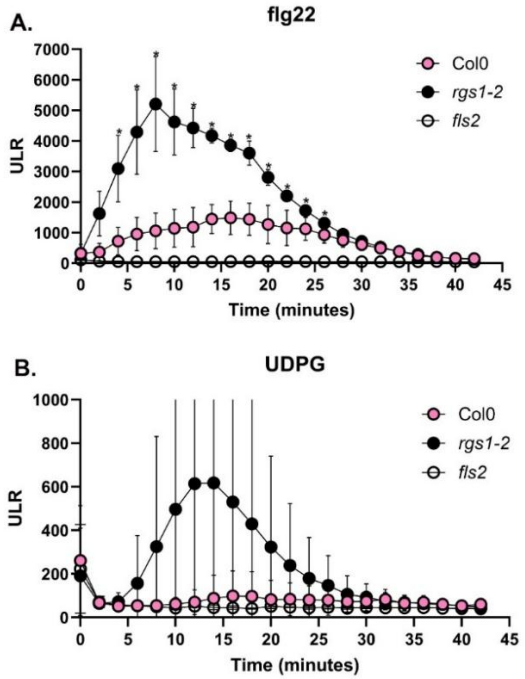


Figure S2. ROS induction by flg22 and UDPG. flg22 (**A**) and UDPG (**B**) induction of ROS over time after application for wild type Col-0 (pink circles), rgs1-2 mutant (black circles), and the negative control, fls2 (open circles). Error bars = StDev. Asterisks represent statistical confidence $p < 0.001$.

Supplementary Information S3. Optimization of time for treatment using flg22-induced ROS production as proxy used in all experiments. This data support conclusions made in the Results section under subsection "Optimization of response time for elicitation". The question of when during a diel cycle should an experiment be conducted was addressed to standardize all the experiments in order to compare the data from individual experiments. In our experience using conditions in our lab, plant sensitivity to flg22 is variable over the time of day. The production of reactive oxygen species (ROS) was used as the proxy for flg22 sensitivity. ROS production was tested by applying 100 nM flg22 to leaf discs that were harvested at different times of the diel cycle imposed by the growth chamber where lights

are on at 9:00 am and off at 5pm (panels A and C). The method used is described by[3]. The results are described in the Methods, section entitled *Optimization of response time for elicitation*.

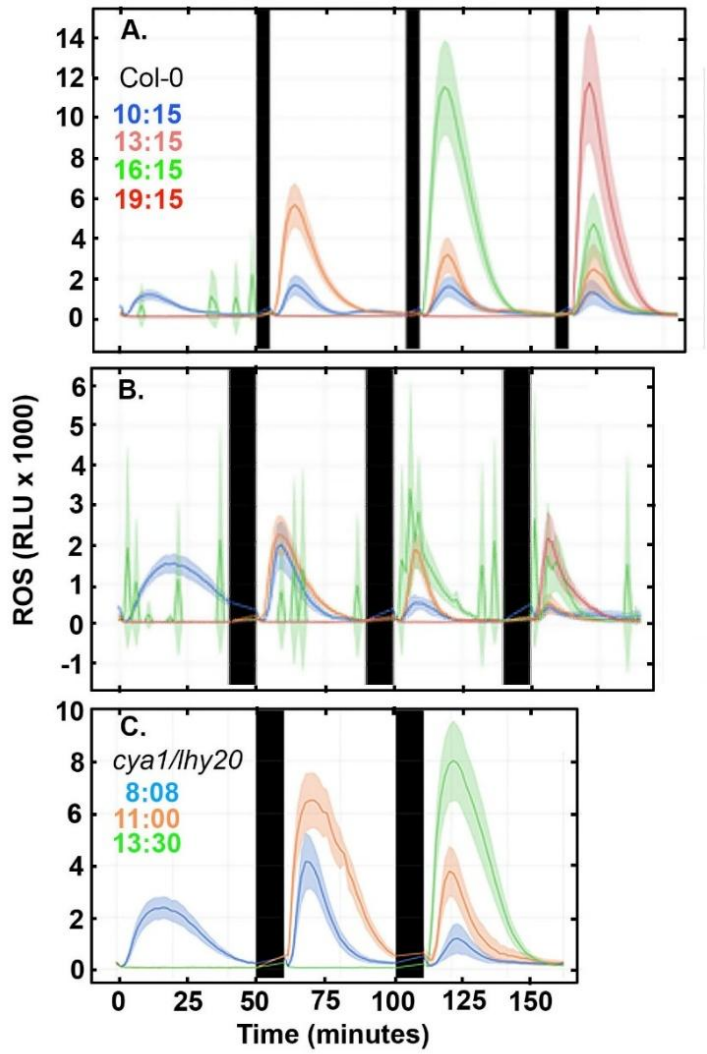


Figure S3. Determining the optimum time of day to conduct the "omics" experiments. ROS was used as the proxy to determine the time of day start experiments. ROS was detected by luminometry. RLU, relative light unit; Col-0, ecotype Columbia zero; (**A**) Col-0 was treated with flg22 at the indicated times for 10 minutes at the indicated times marked by the black bars for plants that had been harvested at the times of 24-h day indicated: blue, 10:15; orange, 13:15; green, 16:15; red, 19:15. (**B**) Plants are grown in a day-night cycle and moved to constant darkness for one day prior to the test period. Same as panel A. (**C**) The circadian clock mutants *cya1* and *lhy20* were combined to completely eliminate the circadian clock. Plants were treated exactly as described for panel A.

Supplemental Information S4. This data support conclusions made in the Methods section, subheading "Optimization of APEX2 labeling over background biotinylation". APEX2, an engineered enzyme derived from soybean ascorbate peroxidase, has been successfully used in a Proximity Labeling (PL) studies in yeast[4] and mammalian cells[5]. APEX2 was engineered to efficiently biotinylate nearby proteins at low levels of enzyme expression using less H_2O_2 and biotin-phenol. An advantage of APEX2 over other peroxidases for PL is that it is the most rapid[4,5]. Given the fast reaction times for flg22 and UDPG on AtRGS1 activation in the range of seconds to minutes, obtaining instantaneous biotin labeling speed is paramount for our experiments. However the usage of APEX2 for plant PL-MS research is disputed because of the poor membrane permeability of biotin phenol, the high abundance of endogenous reactive oxygen species, the high background of biotinylated proteins, and the toxicity of H_2O_2[6-8]. Therefore, considerable optimization preceded sample preparation for MS-MS. Different labeling conditions including different treatment concentration and time of biotin phenol (BP) as well as H_2O_2 in *Arabidopsis* roots. Col-0 wild-type (WT) and *rgs1-2* null mutant expressing 35S::FAPβ-AtRGS1-APEX2 (APEX2 line) were used for the test. We show the results culminating in considerable effort toward this optimization below.

Based on previous studies using APEX2 in yeast mammalian cells[4,5], a BP concentration at 275 μM and a H_2O_2 concentration at 2 mM set our starting point for optimization. After pretreating plant roots with 275 μM BP for 30 minutes, we observed no noticeable difference between WT and APEX2 lines in the absence of H_2O_2 to trigger the labeling reaction (Figure S4A). Upon addition of H_2O_2 for 3 minutes, APEX2 lines showed stronger bands compared to WT. Interestingly, when the labeling reaction was triggered with 2 mM H_2O_2 5 minutes treatment, we observed an unexpected weak band in WT plants (Figure S4A). A similar pattern was seen when the BP pretreatment time was extended to 60 minutes, with the main differences being the appearance of a faint, atypical band in APEX2 lines under 5-minute oxidation with H_2O_2 with a relatively stronger signal intensity (Figure S4B). The stronger bands observed under 3 minutes H_2O_2 treatment indicated that the APEX2 labels proteins, but the unexpected weak bands observed under 5-minute of H_2O_2 suggested that the H_2O_2 treatment concentration or time was too high, possibly damaging roots.

Therefore, the concentration of both BP and H_2O_2 used for the labeling was reduced well beyond published protocols. We saw enhanced band intensity in both WT and APEX2 lines following a 30-minute treatment with 100 μM BP, compared to plants without BP treatment (Figure S4C). This indicates that 30 minutes of 100 μM BP is sufficient for uptake and enables PL in plant cells.

To determine an appropriate H_2O_2 concentration that initiates PL without causing excessive cellular damage, we tested various concentrations. Following a 3-minute treatment with 300 μM H_2O_2, we noticed unexpected banding patterns, with the APEX2 line

showing weaker signals than WT (Figure S4C). Similarly, under 500 µM H_2O_2 for 3 minutes, we observed unusual bands, though in this case, the APEX2 line displayed stronger bands than WT. These results suggest that 300 µM H_2O_2 may cause stress or damage to plant cells, potentially affecting labeling efficiency.

We then tested lower H_2O_2 concentrations (50 µM and 100 µM for 3 minutes) and found no notable differences between WT and APEX2 lines or between mock and treated samples. Based on the expectation that functional APEX2 should generate distinctly stronger labeling in transgenic lines (although not necessarily seen with 1-D SDS-PAGE), we further refined our conditions. Specifically, we treated BP-pretreated (30 min, 100 µM) WT and APEX2 lines with 100 µM H_2O_2 for 30, 60, or 180 seconds, using untreated controls (only BP) for comparison. Encouragingly, under the 30- and 60-second H_2O_2 treatments, APEX2 lines showed clearly stronger bands than WT (Figure S4D). However, the difference was less pronounced at 180 seconds.

This level of optimization yielded a protocol that is much different than published methods thus demonstrating that APEX2 is viable for PL in Arabidopsis. To balance efficient labeling with minimal plant stress, we selected the condition of 30-minute 100 µM BP pretreatment followed by 30-second 100 µM H_2O_2 exposure for all subsequent experiments.

Optimization of PL does not solve the biotinylation background as evident from the PL-MS data. Therefore, to address this problem, APEX2-expressing samples were examined for a systematic enrichment of low p-values. Toward this, a two-sample Kolmogorov-Smirnov (KS) test comparing APEX2 and WT p-value distributions was analyzed. This analysis revealed a highly significant leftward shift in APEX2 p-values, with a D^+= 0.1711, D^- =0.0554, and a p-value less than 2.2^{e-16} (Figure S4E), this strong statistical difference suggests that treatment-induced changes detected in the APEX2 samples were systematically greater than background variation observed in WT controls and provide statistical support for using an empirical p-value threshold to distinguish AtRGS1-associated proximity-labeling signals from background.

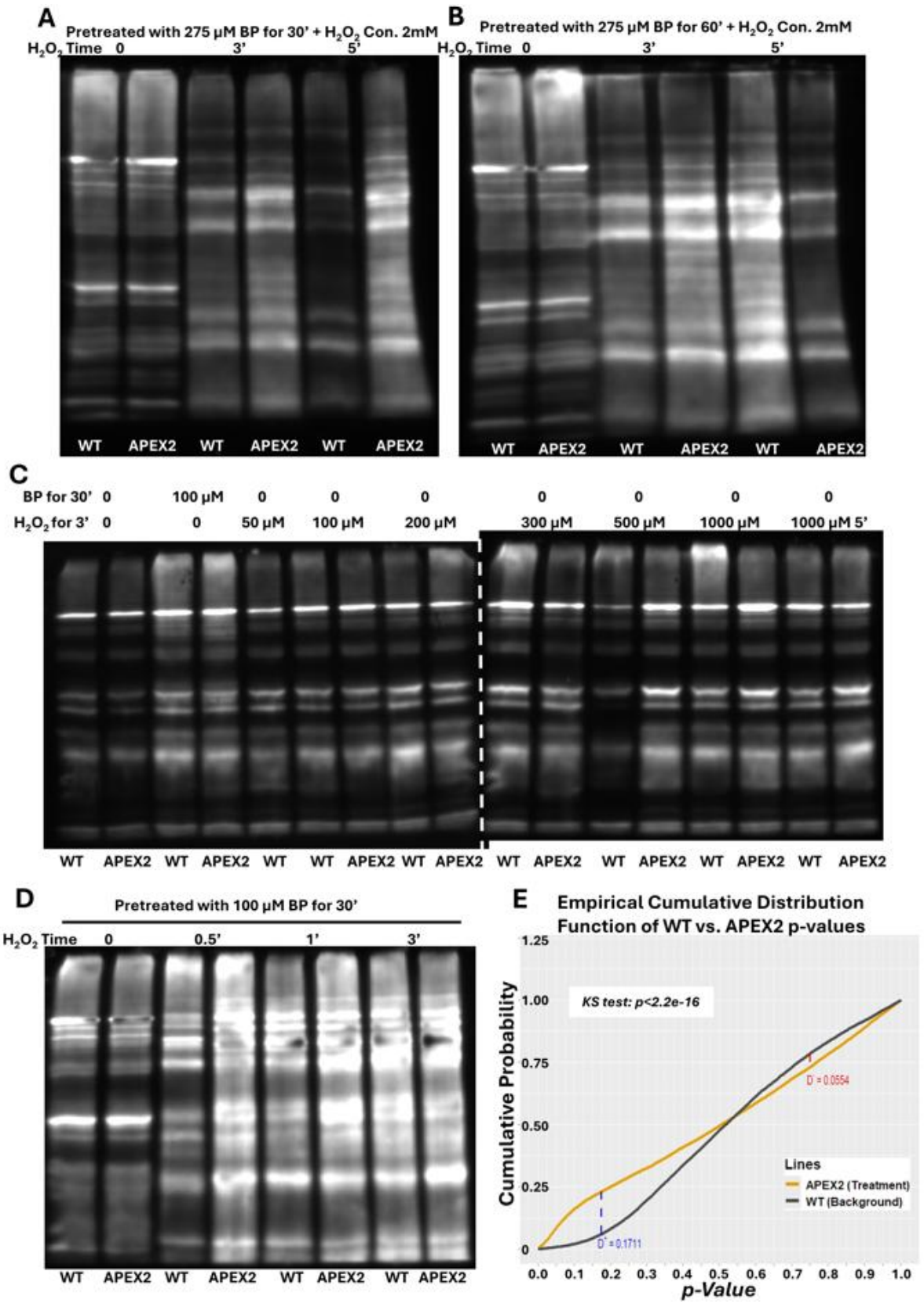

A
Pretreated with 275 μM BP for 30' + H_2O_2 Con. 2mM
H_2O_2 Time 0 3' 5'
WT APEX2 WT APEX2 WT APEX2
B
Pretreated with 275 μM BP for 60' + H_2O_2 Con. 2mM
H_2O_2 Time 0 3' 5'
WT APEX2 WT APEX2 WT APEX2
C
BP for 30' 0 100 μM 0 0 0 0 0 0 0
H_2O_2 for 3' 0 0 50 μM 100 μM 200 μM 300 μM 500 μM 1000 μM 1000 μM 5'
WT APEX2 WT APEX2 WT WT APEX2 WT APEX2 WT APEX2 WT APEX2 WT APEX2 WT APEX2
D
Pretreated with 100 μM BP for 30'
H_2O_2 Time 0 0.5' 1' 3'
WT APEX2 WT APEX2 WT APEX2 WT APEX2
E
Empirical Cumulative Distribution Function of WT vs. APEX2 p-values
KS test: p<2.2e-16
D = 0.0554
D = 0.1711
Lines
APEX2 (Treatment)
WT (Background)
Cumulative Probability
0 0.25 0.50 0.75 1.00 1.25
0.0 0.1 0.2 0.3 0.4 0.5 0.6 0.7 0.8 0.9 1.0
p-Value

Figure S4. Results guiding final selection of the optimal protocol for PL in Arabidopsis roots. (A-D). SDS-PAGE (10% acrylamide) for samples treated as indicated: H_2O_2, hydrogen peroxide time (minutes [panels A-C] or seconds [panel D] as indicated); WT, Col-0 Arabidopsis roots not expressing APEX2; APEX2, Arabidopsis roots expressing AtRGS1 labeled at the C-terminus with APEX2; BP, biotin phenol. Two-weeks old plants were used for the test, and the temperature used for PL test is 22°C. Activity of the APEX2 expressed in *Arabidopsis* was analyzed by immunoblots (IB) with streptavidin-HRP (SA). Lines as well as substrates concentration and treatment time are described in the figure. (A) Pretreatment with 275 µM BP for 30 minutes and activated by 2 mM H_2O_2 for 3 and 5 min per standard protocol. (B) Pretreatment with 275 µM BP for 60 minutes and activated by 2 mM H_2O_2 for 3 and 5 min. (C) Pretreatment with 100 µM BP for 30 minutes and activated by 50-500 µM H_2O_2 for 3 min. (D) Pretreatment with 100 µM BP for 0-180 seconds and activated by 100 µM H_2O_2 for 0-180 seconds. (E) Two-sample Kolmogorov-Smirnov (KS) test comparing APEX2 and WT p-value distributions. X axis is the p-value; y axis is the cumulative probability; p-values from different lines as shown in the figure.

Supplemental Information S5. This data supports construction of AtRGS1-dependent network.

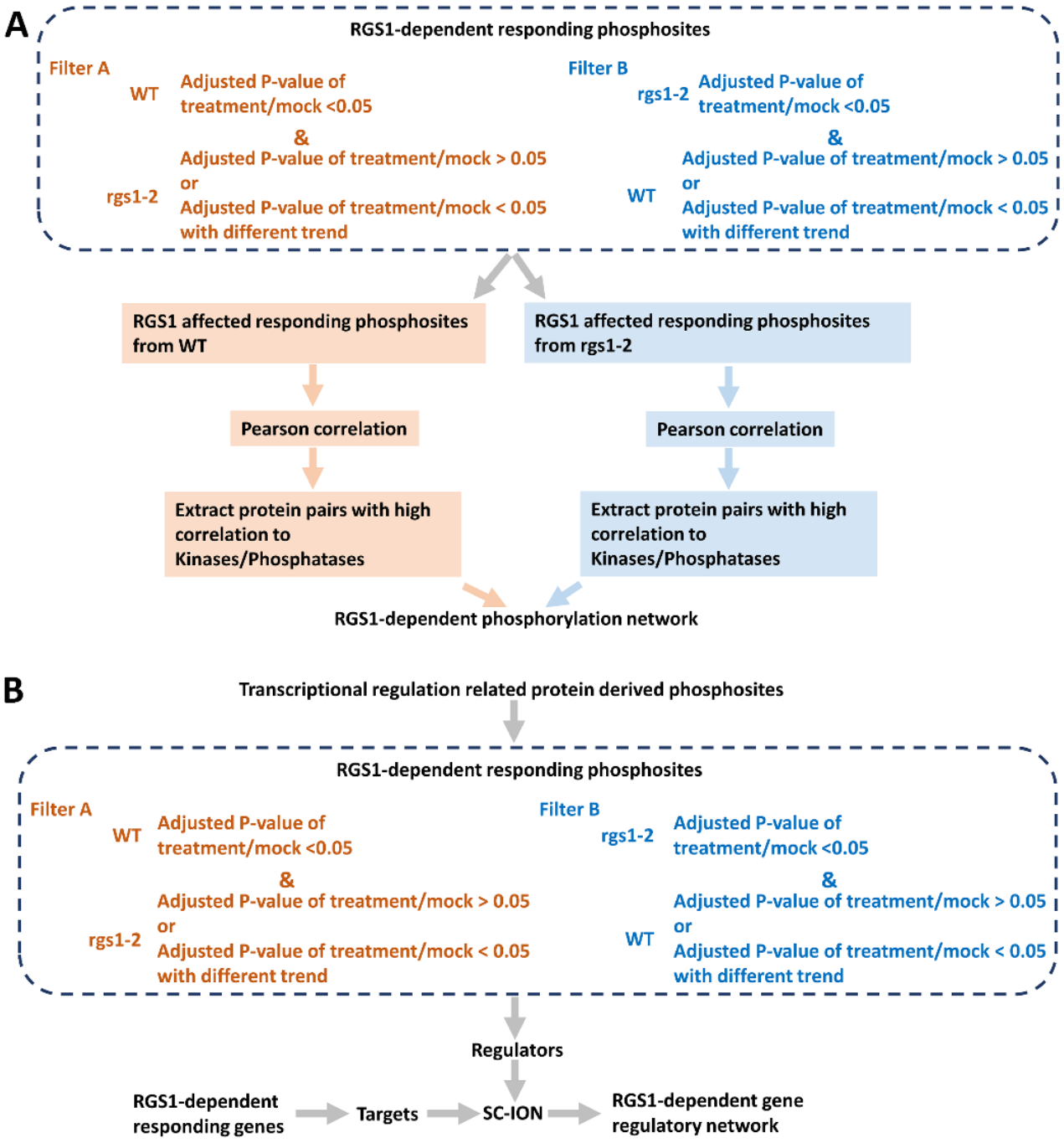


Figure S5. Construction of AtRGS1-dependent network. (A) Construction of AtRGS1-dependent phosphorylation network. AtRGS1-dependent phosphopeptides were identified using two complementary filtering criteria. Filter A selected phosphopeptides that exhibited a significant response (adjusted $P < 0.05$) in WT plants but not in rgs1-2 plants (adjusted $P > 0.05$) under the same treatment condition, or that were significantly regulated

in both genotypes but displayed opposite or divergent response trends. Filter B selected phosphopeptides that exhibited a significant response (adjusted $P < 0.05$) in rgs1-2 plants but not in WT plants (adjusted $P > 0.05$), or that were significantly regulated in both genotypes but showed opposite or divergent response trends. Phosphopeptides that passed either Filter A or Filter B were subjected to Pearson correlation analysis separately in WT and rgs1-2 datasets. Protein pairs with a Pearson correlation coefficient (r) greater than 0.653 were classified as highly correlated. Highly correlated protein pairs involving kinases or phosphatases identified in WT and rgs1-2 plants were combined and used to construct the AtRGS1-dependent phosphorylation network. (B) Construction of the AtRGS1-dependent gene regulatory network. Phosphopeptides derived from transcriptional regulators were filtered for AtRGS1 dependency using Filters A and B, as described in (A), and were used as candidate regulators. AtRGS1-dependent differentially expressed genes identified from the transcriptomic dataset by likelihood ratio testing were used as targets. The regulator and target datasets were integrated into SC-ION to infer regulatory relationships and construct an AtRGS1-dependent gene regulatory network linking phosphorylation events to downstream transcriptional responses.

Supplemental Information S6. This data supports Figure 1. Root growth and gene expression responds to both flg22 an UDPG but with different sensitivities. Seeds were sown on half strength MS medium (1/2 MS) with 0.5% sucrose and 0.7% agar, pH 5.7. After 5 d growth, seedlings were transferred to 1/2 MS containing different concentration of either UDPG or flg22 as described for additional 5 d development. All the plants were grown under 16 h light (day time) 8 h dark (night time), the temperatures for day and night time were 22°C and 20°C separately.

Different patterns of changes in gene expression after UDPG and flg22 treatment roots were observed. The loss of AtRGS1 may have different effects on response to flg22 or UDPG treatment. The expression level of AT5G67160 (ENHANCED PSEUDOMONAS SUSCEPTIBILTY 1, EPS1) was induced upon 1 h 100 nM flg22 treatment in WT plants, but a similar response in *rgs1-2* plants was not detected. AtRGS1 may be involved in activating the expression of EPS1. The expression of genes including AT5G11210 (GLUTAMATE RECEPTOR 2.5, GLR2.5), and AT3G49110 (PEROXIDASE 33, PRX33) were induced upon 1 h 100 nM flg22 treatment and stayed at a high level after 3 h treatment in WT. In *rgs1-2,* the expression of these genes were only found induced upon 3 h 100 nM flg22 treatment, indicating the loss of AtRGS1 may delay the activation of some gene expression. The expression of AT3G50200 in WT was induced after 1 h flg22 treatment but showed no statistical difference between 3 h and no treatment, however *rgs1-2* showed induced expression of this gene under both 1 h and 3 h treatment. This suggests that AtRGS1 plays a role in negative feedback in gene expression. Compared to AT3G50200, the expression of AT1G07400 (HSP20-like chaperones superfamily protein, HSP17.8) was induced in WT plants under both 1 h, 3 h, and in *rgs1-2* plants under 1 h treatment. AtRGS1 may be involved in positive feedback in gene expression. The loss of AtRGS1 may result in statistically differential expression of genes under 1 h and 3 h flg22 treatment (AT1G71380, GLYCOSYL HYDROLASE 9B3), or under 1 h and 3 h UDPG treatment (AT3G28360, ATP-BINDING CASSETTE B16). WT plants did not show a statistical difference when comparing treated

to no treated. The expression of AT1G21528 in WT was slightly induced when treated with 1 h flg22, and showed a statistical difference after 3 h flg22 treatment. But 1 h flg22 treatment depressed the expression of this gene in *rgs1*-2, and 3 h flg22 induced it just as in WT plants.

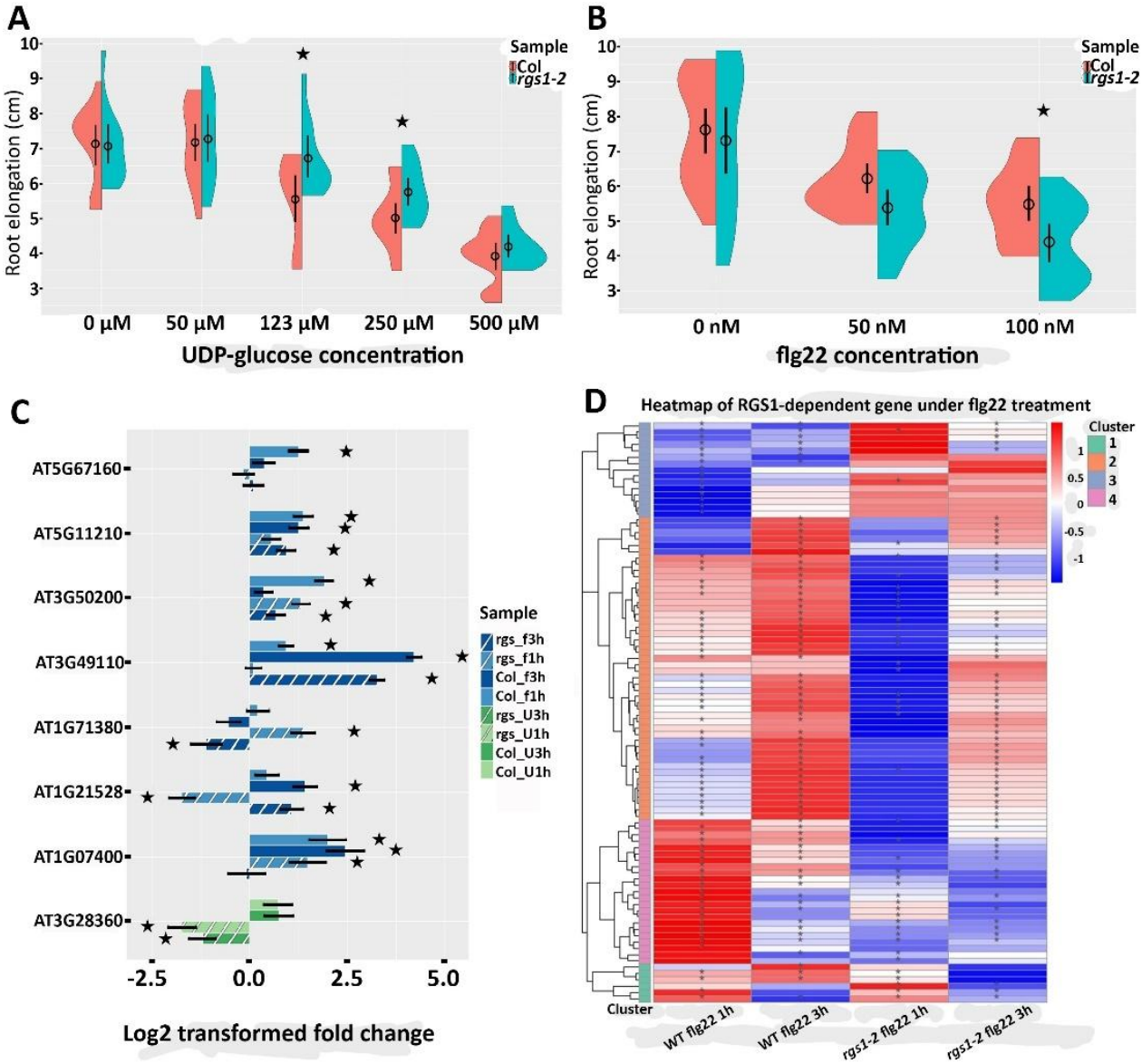


Figure S6. WT and *rgs1-2* root elongation respond to external UDPG and flg22 but with different sensitivities. Root elongation in the presence of UDPG (**A**) or flg22 (**B**) Circle: Mean value, Error bar: Standard deviation. T-test with BH adjustment was chosen for statistics significant study, significant difference as indicted with star. (**C**) Eight bins for different patterns of changes in gene expression after UDPG and flg22 treatment roots occur for which a representative gene in each group is shown. The ATG gene identifier is shown for that representative gene. Log2 fold change (L2FC) of genes that are involved in AtRGS1 dependent responses to flg22 or UDPG. Bars without any pattern are genes from Col plants; Bars with patterns inside are genes from *rgs1-2* plants; light blue is L2FC between 1 h 100 nM flg22 treated group and none treatment group; dark blue is L2FC

between 3 h 100 nM flg22 treated group and none treatment group; light green is L2FC between 1 hour 123 μM UDPG treated group and none treatment group; dark green is L2FC between 3 hour 123 μM UDPG treated group and no treatment group; asterisk indicates statistically different (adjusted p-value less than 0.05); statistics analysis was done with Wald test, and Benjamini-Hochberg procedure was used for multiple comparison adjustment. (**D**) Heatmap of AtRGS1 dependent genes respond to flg22 treatment. WT flg22 1h means log2 fold change of genes from WT plants between 1 hour 100 nM flg22 treatment and WT mock group; WT flg22 3h means log2 fold change of genes from WT plants between 3 hour 100 nM flg22 treatment and WT mock group; *rgs1-2* flg22 1h means log2 fold change of genes from *rgs1-2* plants between 1 h 100 nM flg22 treatment and *rgs1-2* mock group; *rgs1-2* flg22 3h means log2 fold change of genes from *rgs1-2* plants between 3 hour 100 nM flg22 treatment and *rgs1-2* mock group; different clusters were labeled with corresponding numbers 1-4; asterisks indicate BH adjusted p-value less than 0.05; fold change as indicate in scale bar.

Supplemental Information S7. This data supports data shown in Figure 3E. This figure contains all proteins found in the AtRGS1-dependent phosphorylation network

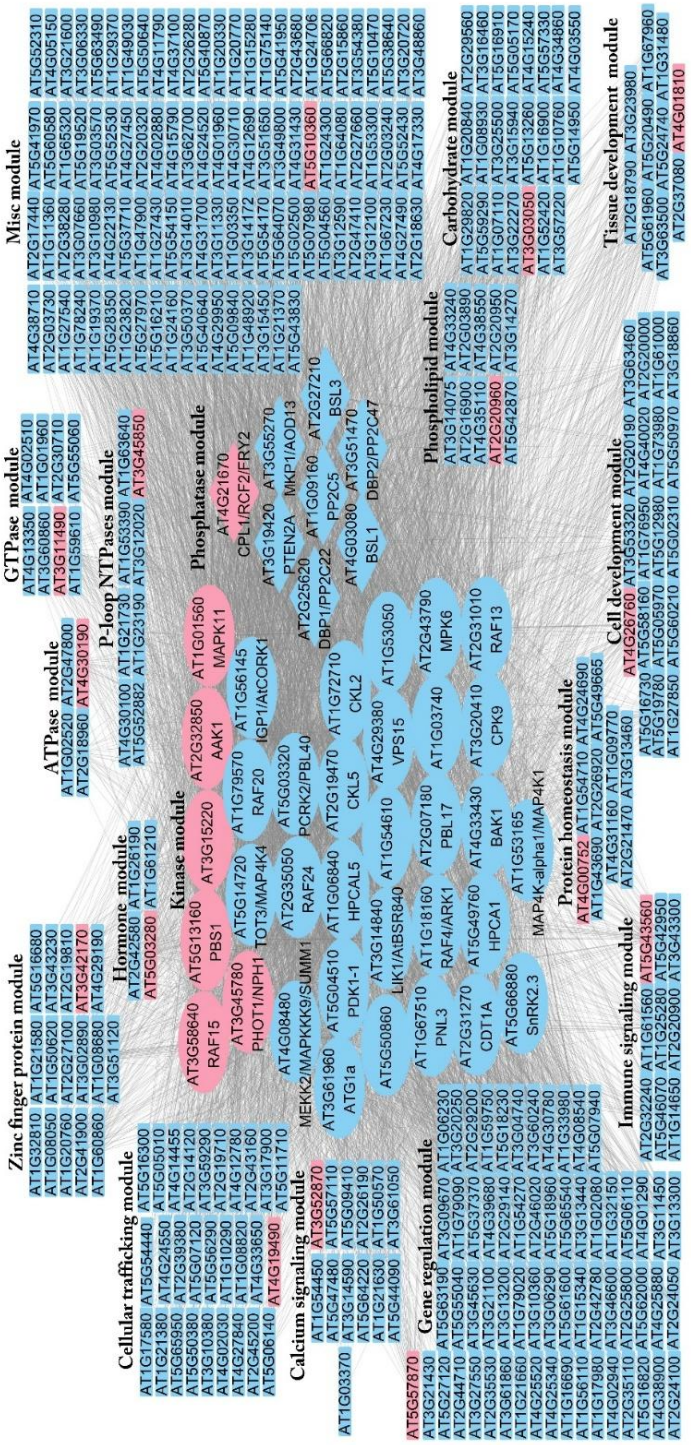


Figure S7. AtRGS1-dependent phosphorylation network. Eclipse shows protein kinase, diamond shows protein phosphatase, square shows correlated protein of kinase or phosphatase. All proteins within the network were grouped into different modules as shown in the figure according to their functions. Proteins with high edge count or neighborhood connectivity within each module were highlighted in purple.

Supplemental Information S8. This data supports AtRGS1 phospho-bar code

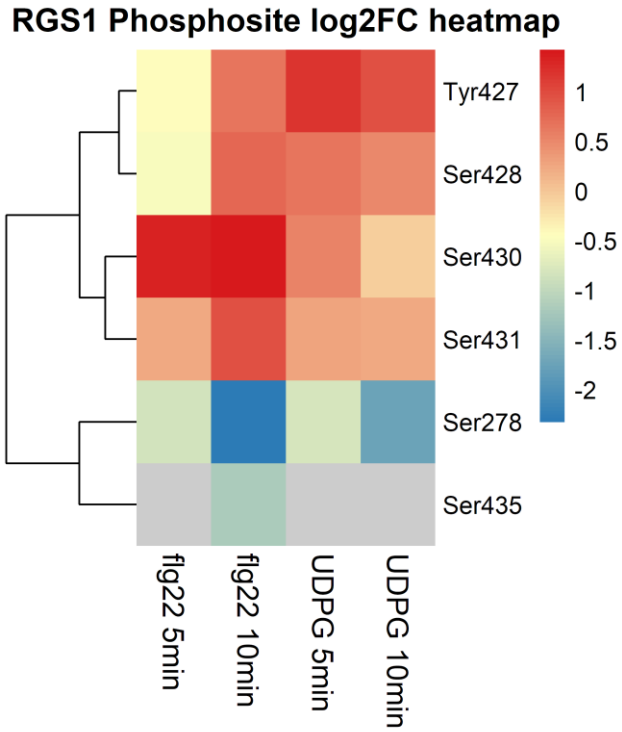


Figure S8. AtRGS1 phospho-bar code. Phosphosites of AtRGS1 were detected with DIA base phosphoproteome. Phosphosites with a phosphorylation site localization probability higher than 0.05 were chosen for further analysis. Log2 fold change (log2FC) of phosphosites were calculated using treatment (as indicated by x-axis label) vs mock. Phosphosites with similar trend were clustered.

Supplemental Information S9. This data supports conclusions made in the Discussion section. To reconstruct the AtRGS1 mediated signaling pathway responds to flg22, we constructed a network incorporating transcription related proteins identified from AtRGS1-dependent phosphosites and AtRGS1-dependent genes from transcriptome data using SCION[9,10].

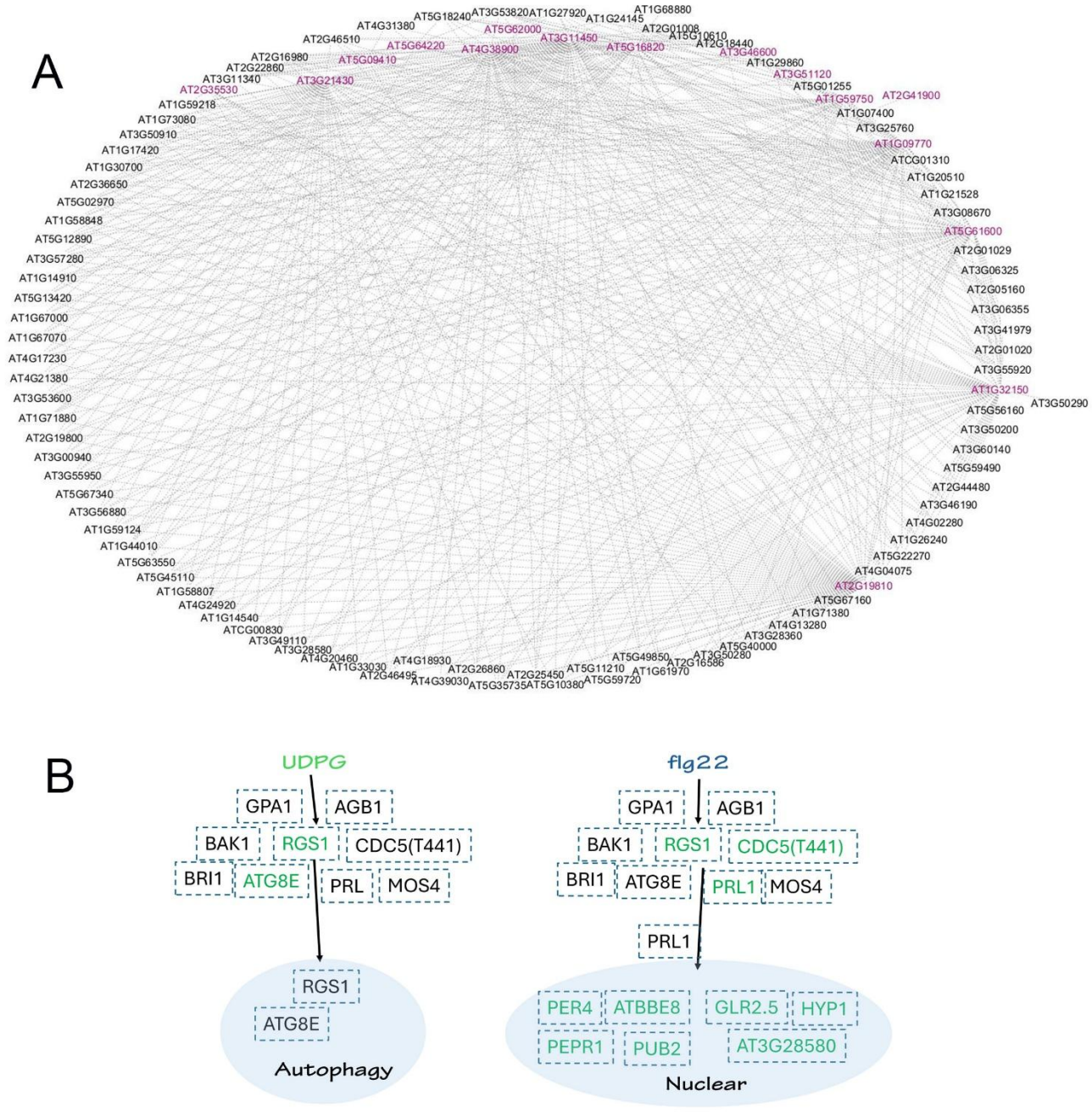


Figure S9. AtRGS1-mediated phosphoproteome to transcriptome network responds to flg22 and biased signaling pathway responding to UDPG and flg22. (A) AtRGS1-mediated phosphoproteome to transcriptome network responds to flg22. Transcription

related proteins containing AtRGS1-dependent phosphosites from phosphoproteome and AtRGS1-dependent genes from transcriptome data were chosen for SCION[9,10] analysis. And correlations with strong strength were chosen for construction of panel A, transcription related proteins were in purple, AtRGS1-dependent genes were in black, the interaction was indicated as dot line. (B) Circuit model with AtRGS1 as the core, left demonstrates how AtRGS1 core responds to UDPG, right demonstrates how AtRGS1 core responds to flg22.

Table S1

Motif	Motif Type	Enriched in Cluster	Adjusted p-value	Score	Target for Kinase
xxxxxxx_**S**_Pxxxxxx	**SP**	1	2.40E-16	42.4	MPK, SnRK2, RLK, AGC, CDK, CDPK, SLK
xxxxxxx_**S**_Pxxxxxx		2	5.20E-08	23.77	
xxxxRxx_**S**_xxxxxxx	**R**xx**S**		3.00E-02	7.68	SnRK2, CDPK
xxxSxxx_**S**_Pxxxxxx	**SP**	3	4.30E-05	37.15	MPK, SnRK2, RLK, AGC, CDK, CDPK, SLK
xxxxxxx_**S**_Pxxxxxx			1.10E-12	17.72	
xxxxxxx_**S**_Pxxxxxx	**SP**	4	1.80E-12	28.09	MPK, SnRK2, RLK, AGC, CDK, CDPK, SLK

Table S2

Treatment & trend	Proximity labeling	Pull down	Shared
flg22 5 min down regulated	248	0	0
flg22 5 min up regulated	33	0	0
flg22 10 min down regulated	258	2	1
flg22 10 min up regulated	17	0	0
UDPG 5 min down regulated	61	830	8
UDPG 5 min up regulated	29	6	0
UDPG 10 min down regulated	2728	933	616
UDPG 10 min up regulated	1	4	0

REFERENCES FOR SUPPLEMENTAL INFORMATION

1. Jia, H., Lou, F., Watkins, J., Oliveira, C.C., Tate, C.G., and Jones, A.M. (2025). UDP-glucose Activation of a G-protein/Sucrose Synthase Signaling Supercomplex. bioRxiv, 2025.2009. 2010.672744.
2. Watkins, J.M., Montes, C., Clark, N.M., Song, G., Oliveira, C.C., Mishra, B., Brachova, L., Seifert, C.M., Mitchell, M.S., and Yang, J. (2024). Phosphorylation Dynamics in a flg22-Induced, G Protein–Dependent Network Reveals the AtRGS1 Phosphatase. Molecular & Cellular Proteomics *23*.
3. Ghusinga, K.R., Paredes, F., Jones, A.M., and Colaneri, A. (2021). Reported differences in the flg22 response of the null mutation of AtRGS1 correlates with fixed genetic variation in the background of Col-0 isolates. Plant Signaling & Behavior *16*, 1878685.
4. Singer-Krüger, B., Fröhlich, T., Franz-Wachtel, M., Nalpas, N., Macek, B., and Jansen, R.P. (2020). APEX2-mediated proximity labeling resolves protein networks in Saccharomyces cerevisiae cells. The FEBS Journal *287*, 325-344.
5. Del Olmo, T., Lauzier, A., Normandin, C., Larcher, R., Lecours, M., Jean, D., Lessard, L., Steinberg, F., Boisvert, F.M., and Jean, S. (2019). APEX2-mediated RAB proximity labeling identifies a role for RAB21 in clathrin-independent cargo sorting. EMBO reports *20*, e47192.
6. Mair, A., and Bergmann, D.C. (2022). Advances in enzyme-mediated proximity labeling and its potential for plant research. Plant Physiology *188*, 756-768.
7. Samavarchi-Tehrani, P., Samson, R., and Gingras, A.-C. (2020). Proximity dependent biotinylation: key enzymes and adaptation to proteomics approaches. Molecular & Cellular Proteomics *19*, 757-773.
8. Xu, S.-L., Shrestha, R., Karunadasa, S.S., and Xie, P.-Q. (2023). Proximity labeling in plants. Annual review of plant biology *74*, 285-312.
9. Clark, N. (2023). nmclark2/SCION: Version 4.1 (Zenodo).
10. Clark, N.M., Nolan, T.M., Wang, P., Song, G., Montes, C., Valentine, C.T., Guo, H., Sozzani, R., Yin, Y., and Walley, J.W. (2021). Integrated omics networks reveal the temporal signaling events of brassinosteroid response in Arabidopsis. Nature Communications *12*, 5858.